

Two Higgs doublet model with a complex singlet scalar and Multi-critical Point Principle

Gi-Chol Cho^{1,*}, Chikako Idegawa^{2,†} and Chiaki Nose^{3‡}

¹*Department of Physics, Ochanomizu University, Tokyo 112-8610, Japan*

² *MOE Key Laboratory of TianQin Mission,
TianQin Research Center for Gravitational Physics & School of Physics and Astronomy,
Frontiers Science Center for TianQin,
Gravitational Wave Research Center of CNSA,
Sun Yat-sen University (Zhuhai Campus), Zhuhai 519082, China and*

³*Graduate school of Humanities and Sciences,
Ochanomizu University, Tokyo 112-8610, Japan*

(Dated: January 7, 2026)

Abstract

We study a two Higgs doublet model extended by a complex singlet scalar, in which the imaginary part of the singlet serves as a dark matter (DM) candidate. In this model, degenerate masses of the three neutral Higgs bosons are crucial for achieving consistency with current constraints from DM direct-detection experiments and Higgs searches. This is called the degenerate scalar scenario. To provide a theoretical motivation for such a degenerate Higgs spectrum, we impose the tree-level Multiple Point Principle (MPP), which requires the electroweak and singlet vacua to be degenerate, and analyze its implications for the scalar potential, DM phenomenology, and the electroweak phase transition. We show that the tree-level MPP favors large $SU(2)_L$ doublet-singlet mixing parameters, which compete with the degenerate scalar scenario. Nevertheless, we demonstrate that viable parameter regions still exist in which the observed DM constraints are satisfied. Furthermore, although the tree-level MPP forbids a tree-level-driven first-order electroweak phase transition, we show that thermal loop effects can induce a strong first-order transition compatible with electroweak baryogenesis.

* cho.gichol@ocha.ac.jp

† idegawa@mail.sysu.edu.cn

‡ chiaki.nose@hep.phys.ocha.ac.jp

I. INTRODUCTION

The discovery of the Higgs boson in 2012 completed the Standard Model (SM) as a renormalizable quantum field theory describing electroweak symmetry breaking [1, 2]. Nevertheless, the structure of the Higgs sector itself remains one of the most intriguing open questions in particle physics. Among various extensions of the SM, the two Higgs doublet model (2HDM) is one of the simplest and most motivated frameworks [3–6]. However, the general form of the 2HDM does not provide a viable dark matter (DM) candidate, whereas the existence of DM has been firmly established by cosmological and astrophysical observations and cannot be explained within the SM.

To accommodate a DM candidate, we extend the 2HDM by introducing an additional complex singlet scalar field S [7–10]. We refer to this model as 2HDMS. In the 2HDMS, the imaginary part of the singlet behaves as a weakly interacting massive particle (WIMP) DM. In addition, the neutral components of the two Higgs doublets and the real part of S mix to form three Higgs bosons $H_{1,2,3}$. Recent direct detection experiments, such as the LUX-ZEPLIN (LZ) experiment [11], have placed stringent constraints on WIMP dark matter. In this model, the elastic scattering between the DM particle and nucleons is mediated by three Higgs bosons. Interestingly, the scattering cross section can be naturally suppressed when the Higgs masses are nearly degenerate [12]. This mechanism, known as the degenerate scalar scenario, provides a theoretically consistent explanation for the null results of direct detection experiments.

In previous studies, such mass degeneracy among scalars was introduced by hand. In this work, we seek a principle that determines the scalar potential parameters and simultaneously realizes mass degeneracy. For this purpose, we adopt the Multiple Point Principle (MPP) [13–15] as a guiding principle. Originally, the MPP was proposed as a condition requiring the coexistence of multiple vacua with identical energy densities — typically between the electroweak and a high-energy scale vacua — and has successfully predicted the Higgs boson mass within the SM [16]. In the present model, however, the scalar potential naturally possesses two distinct vacua at the low-energy scale: one along the electroweak direction and the other along the singlet direction. The authors of ref. [17] argue that, if the MPP is a fundamental principle, it should be imposed on all possible vacua, including those dominated by the tree-level potential in models with extended scalar sectors. We therefore

consider the case in which these two vacua are degenerate and refer to this condition as the tree-level MPP. Such a setup not only provides an origin for the degenerate scalar scenario but also has important implications for the electroweak phase transition (EWPT) [18]. For a recent study, see ref. [19].

We analyze the conditions imposed on the model parameters by the tree-level MPP and, at the same time, explore the parameter regions favored by the DM relic density and direct detection constraints. Particular attention is paid to the mixing terms between the Higgs doublets and the singlet scalar, which play essential roles in both the MPP condition and the DM phenomenology, affecting the two in opposite directions. We show that, even under these mutually competing constraints, there still exists an allowed parameter space where both conditions can be satisfied simultaneously.

On the other hand, once the tree-level MPP is imposed, the potential barrier relevant to the EWPT is not generated at tree level, and only one-loop thermal effects are responsible for its formation. We demonstrate that, even under the tree-level MPP, a strong first-order EWPT required for successful electroweak baryogenesis can occur purely due to thermal loop effects.

The structure of this paper is as follows. In Sec. II, we introduce the 2HDMs and define the scalar potential, mass spectrum, and relevant interactions. In Sec. III, we impose the tree-level MPP and discuss its implications for the vacuum structure and the EWPT. In Sec. IV, we study the DM phenomenology, focusing on the relic abundance and direct-detection constraints using representative benchmark points favored by the tree-level MPP. Finally, Sec. V is devoted to a summary and conclusions.

II. THE COMPLEX SINGLET EXTENDED HIGGS MODEL

A. Model

In the 2HDMs, the tree-level scalar potential V_0 is given by

$$V_0 = V_{0,2\text{HDM}} + V_{0,\text{S}}. \quad (1)$$

The first term on the right-hand side of Eq. (1) involves only the two Higgs doublet fields, Φ_1 and Φ_2 :

$$\begin{aligned} V_{0,2\text{HDM}}(\Phi_1, \Phi_2) &= m_1^2 \Phi_1^\dagger \Phi_1 + m_2^2 \Phi_2^\dagger \Phi_2 - \left(m_3^2 \Phi_1^\dagger \Phi_2 + \text{h.c.} \right) \\ &+ \frac{\lambda_1}{2} (\Phi_1^\dagger \Phi_1)^2 + \frac{\lambda_2}{2} (\Phi_2^\dagger \Phi_2)^2 + \lambda_3 (\Phi_1^\dagger \Phi_1)(\Phi_2^\dagger \Phi_2) \\ &+ \lambda_4 (\Phi_1^\dagger \Phi_2)(\Phi_2^\dagger \Phi_1) + \left[\frac{\lambda_5}{2} (\Phi_1^\dagger \Phi_2)^2 + \text{h.c.} \right], \end{aligned} \quad (2)$$

where only the m_3^2 term softly breaks the Z_2 symmetry of the doublets ($\Phi_1 \rightarrow +\Phi_1$, $\Phi_2 \rightarrow -\Phi_2$). The second term in Eq. (1), involving the singlet field S and the doublets, is given by

$$\begin{aligned} V_{0,S}(\Phi_1, \Phi_2, S) &= \frac{\delta_1}{2} \Phi_1^\dagger \Phi_1 |S|^2 + \frac{\delta_2}{2} \Phi_2^\dagger \Phi_2 |S|^2 + \frac{b_2}{2} |S|^2 + \frac{d_2}{4} |S|^4 \\ &+ \left(a_1 S + \frac{b_1}{4} S^2 + \text{h.c.} \right), \end{aligned} \quad (3)$$

where the terms in the first line are invariant under a global U(1) transformation $S \rightarrow e^{i\theta}S$, while those in the second line softly break this symmetry. In the following, all coefficients in the scalar potential are taken to be real.

The Higgs doublets Φ_i ($i = 1, 2$) and the singlet S are expanded around their vacuum expectation values (VEVs) as

$$\Phi_i = \begin{pmatrix} \phi_i^+ \\ \frac{1}{\sqrt{2}}(v_i + h_i + i\eta_i) \end{pmatrix}, \quad S = \frac{1}{\sqrt{2}}(v_S + s + i\chi). \quad (4)$$

Here $v \equiv \sqrt{v_1^2 + v_2^2} = 246.22$ GeV and $\tan \beta \equiv v_2/v_1$. The components of Φ_i and S consist of charged scalars (ϕ_i^+), neutral scalar components (h_1, h_2, s), and neutral pseudoscalar components (η_i, χ). The field χ is stable and serves as the DM candidate. The first derivatives of V_0 with respect to h_1 , h_2 , and s yield the following tadpole conditions:

$$\left\langle \frac{\partial V_0}{\partial h_1} \right\rangle = m_1^2 v_1 - m_3^2 v_2 + \frac{\lambda_1}{2} v_1^3 + \frac{\lambda_{345}}{2} v_1 v_2^2 + \frac{\delta_1}{4} v_1 v_S^2 = 0, \quad (5)$$

$$\left\langle \frac{\partial V_0}{\partial h_2} \right\rangle = m_2^2 v_2 - m_3^2 v_1 + \frac{\lambda_2}{2} v_2^3 + \frac{\lambda_{345}}{2} v_1^2 v_2 + \frac{\delta_2}{4} v_2 v_S^2 = 0, \quad (6)$$

$$\left\langle \frac{\partial V_0}{\partial s} \right\rangle = \sqrt{2} a_1 + \frac{b_1 + b_2}{2} v_S + \frac{\delta_1}{4} v_1^2 v_S + \frac{\delta_2}{4} v_2^2 v_S + \frac{d_2}{4} v_S^3 = 0, \quad (7)$$

where $\lambda_{345} = \lambda_3 + \lambda_4 + \lambda_5$.

The mass matrix for the neutral scalar components is obtained as

$$-\mathcal{L}_{\text{mass}} = \frac{1}{2} \begin{pmatrix} h_1 & h_2 & s \end{pmatrix} \mathcal{M}_S^2 \begin{pmatrix} h_1 \\ h_2 \\ s \end{pmatrix} = \frac{1}{2} \begin{pmatrix} H_1 & H_2 & H_3 \end{pmatrix} O^\top \mathcal{M}_S^2 O \begin{pmatrix} H_1 \\ H_2 \\ H_3 \end{pmatrix} = \frac{1}{2} \sum_{i=1}^3 m_{H_i}^2 H_i^2, \quad (8)$$

where

$$\mathcal{M}_S^2 = \begin{pmatrix} m_3^2 \frac{v_2}{v_1} + \lambda_1 v_1^2 & -m_3^2 + \lambda_{345} v_1 v_2 & \frac{\delta_1}{2} v_1 v_S \\ -m_3^2 + \lambda_{345} v_1 v_2 & m_3^2 \frac{v_1}{v_2} + \lambda_2 v_2^2 & \frac{\delta_2}{2} v_2 v_S \\ \frac{\delta_1}{2} v_1 v_S & \frac{\delta_2}{2} v_2 v_S & -\frac{\sqrt{2} a_1}{v_S} + \frac{d_2}{2} v_S^2 \end{pmatrix}. \quad (9)$$

The orthogonal matrix O diagonalizes \mathcal{M}_S^2 and can be parametrized as

$$O(\alpha_i) = \begin{pmatrix} 1 & 0 & 0 \\ 0 & c_3 & -s_3 \\ 0 & s_3 & c_3 \end{pmatrix} \begin{pmatrix} c_2 & 0 & -s_2 \\ 0 & 1 & 0 \\ s_2 & 0 & c_2 \end{pmatrix} \begin{pmatrix} c_1 & -s_1 & 0 \\ s_1 & c_1 & 0 \\ 0 & 0 & 1 \end{pmatrix}, \quad (10)$$

where $s_i = \sin \alpha_i$ and $c_i = \cos \alpha_i$ ($i = 1, 2, 3$). The orthogonality condition is given by

$$\sum_k O_{ik} O_{jk} = \delta_{ij}. \quad (11)$$

The three mass eigenstates $H_{1,2,3}$ correspond to the physical neutral Higgs bosons, where H_1 is identified with the observed 125 GeV Higgs at the LHC. On the other hand, the charged scalar H^\pm and the pseudoscalar A are defined from $\phi_{1,2}^+$ and $\eta_{1,2}$ as

$$\begin{pmatrix} \phi_1^+ \\ \phi_2^+ \end{pmatrix} = R(\beta) \begin{pmatrix} G^+ \\ H^+ \end{pmatrix}, \quad \begin{pmatrix} \eta_1 \\ \eta_2 \end{pmatrix} = R(\beta) \begin{pmatrix} G^0 \\ A \end{pmatrix}, \quad (12)$$

with

$$R(\beta) = \begin{pmatrix} \cos \beta & -\sin \beta \\ \sin \beta & \cos \beta \end{pmatrix}. \quad (13)$$

Here G^\pm and G^0 denote the Nambu-Goldstone bosons. The corresponding mass eigenvalues are given by

$$m_{H^\pm}^2 = \frac{m_3^2}{\sin \beta \cos \beta} - \frac{1}{2}(\lambda_4 + \lambda_5)v^2, \quad (14)$$

$$m_A^2 = \frac{m_3^2}{\sin \beta \cos \beta} - \lambda_5 v^2, \quad (15)$$

Inputs	$v, v_S, m_{H_1}, m_{H_2}, m_{H_3}, m_{H^\pm}, m_A, m_\chi, \alpha_1, \alpha_2, \alpha_3, \tan \beta, m_3^2, a_1$
Outputs	$v_1, v_2, m_1^2, m_2^2, \lambda_1, \lambda_2, \lambda_3, \lambda_4, \lambda_5, \delta_1, \delta_2, b_2, d_2, b_1$

TABLE I. Input and output parameters in this model.

and the DM mass is

$$m_\chi^2 = -\frac{\sqrt{2}a_1}{v_S} - b_1. \quad (16)$$

Let us summarize the input parameters and several theoretical constraints. The scalar potential contains 14 parameters $\{m_1^2, m_2^2, m_3^2, \lambda_1, \lambda_2, \lambda_3, \lambda_4, \lambda_5, \delta_1, \delta_2, b_2, d_2, a_1, b_1\}$. Among them, $\{m_3^2, a_1\}$ are treated as free input parameters, while the remaining 12 parameters are output parameters. The parameters $\{m_1^2, m_2^2, b_2\}$ are determined by the tadpole conditions (5)–(7), and $\{\lambda_4, \lambda_5, b_1\}$ are fixed by the physical masses in Eqs. (14)–(16). The remaining six parameters are determined from the neutral scalar mass matrix. The input and output parameters are summarized in Table I.

Since δ_1 , δ_2 , and d_2 play a central role in the discussion of the phase transition, we display their explicit expressions here:

$$\delta_1 = \frac{2}{v_1 v_S} \sum_{i=1}^3 O_{1i} O_{3i} m_{H_i}^2, \quad (17)$$

$$\delta_2 = \frac{2}{v_2 v_S} \sum_{i=1}^3 O_{2i} O_{3i} m_{H_i}^2, \quad (18)$$

$$d_2 = \frac{2}{v_S^2} \left(\frac{\sqrt{2} a_1}{v_S} + \sum_{i=1}^3 O_{3i}^2 m_{H_i}^2 \right). \quad (19)$$

These relations will be relevant when discussing both the MPP condition and the structure of the EWPT. All remaining relations between the physical inputs and the original Lagrangian parameters are summarized in Appendix A.

The scalar potential is required to be bounded from below, leading to the conditions [20, 21]

$$\lambda_1 > 0, \quad \lambda_2 > 0, \quad \lambda_3 + \lambda_4 - \lambda_5 > -\sqrt{\lambda_1 \lambda_2}, \quad d_2 > 0. \quad (20)$$

The quartic couplings are further constrained by tree-level unitarity [22–26]:

$$\lambda_1 < \frac{8\pi}{3}, \quad \lambda_2 < \frac{8\pi}{3}, \quad \lambda_{345} < 8\pi, \quad \delta_1 < 16\pi, \quad \delta_2 < 16\pi, \quad d_2 < \frac{16\pi}{3}. \quad (21)$$

	Q_L, L_L	u_R	d_R	ℓ_R	Φ_u	Φ_d	Φ_ℓ
Type-I	+	–	–	–	Φ_2	Φ_2	Φ_2
Type-II	+	–	+	+	Φ_2	Φ_1	Φ_1
Type-X	+	–	–	+	Φ_2	Φ_2	Φ_1
Type-Y	+	–	+	–	Φ_2	Φ_1	Φ_2

TABLE II. Assignments of Z_2 charges to the fermions and the corresponding Higgs doublets that couple to each fermion type. The Higgs doublets transform as $\Phi_1 \rightarrow +\Phi_1$ and $\Phi_2 \rightarrow -\Phi_2$, respectively.

Perturbativity additionally requires [27]

$$|\lambda_i|, d_2 < 4\pi \quad (i = 1-5). \quad (22)$$

To avoid tree-level flavor-changing neutral currents (FCNCs), we assume that each type of fermion couples to only one of the Higgs doublets [4, 28]. The Yukawa Lagrangian is written as

$$-\mathcal{L}_{\text{Yukawa}} = \bar{Q}_L Y_u \tilde{\Phi}_u u_R + \bar{Q}_L Y_d \Phi_d d_R + \bar{L}_L Y_\ell \Phi_\ell \ell_R + \text{h.c.}, \quad (23)$$

where Φ_f ($f = u, d, \ell$) is the Higgs doublet that couples to fermion f , $\tilde{\Phi}_u \equiv i\sigma_2 \Phi_u^*$, and σ_2 is the Pauli matrix. Here $Q_L = (u_L, d_L)^\top$ and $L_L = (\nu_L, e_L)^\top$ represent the left-handed quark and lepton doublets, respectively, while u_R , d_R , and ℓ_R are the corresponding right-handed singlets. Y_f ($f = u, d, \ell$) denote the 3×3 Yukawa coupling matrices. As summarized in Table II, by assigning appropriate Z_2 charges to the fermions, one can identify which Higgs doublet couples to each fermion type, leading to four distinct Yukawa structures.

B. Degenerate scalar scenario

Recent DM direct detection experiments have provided stringent upper limits on the spin-independent DM–nucleon scattering cross section [11], which strongly constrain various Higgs-portal-type DM models. In the 2HDMS, the elastic scattering between the DM particle χ and nucleons is mediated by the three neutral Higgs bosons H_i ($i = 1, 2, 3$). The relevant process is

$$\chi(p_1) + q(p_2) \rightarrow \chi(p_3) + q(p_4), \quad (24)$$

which proceeds through the t -channel exchange of H_1 , H_2 , and H_3 .

As an illustrative example, we consider the Type-I 2HDMs, in which all fermions couple only to the Higgs doublet Φ_2 . The couplings between the up-type and the down-type quark u, d and the mass eigenstates H_i are therefore written as

$$-\mathcal{L}_{\text{Yukawa}} = \sum_{i=1}^3 C_{uuH_i} \bar{u}_L u_R H_i + \sum_{i=1}^3 C_{ddH_i} \bar{d}_L d_R H_i + \text{h.c.}, \quad (25)$$

with

$$C_{uuH_i} = \frac{m_u}{v_2} O_{2i}, \quad C_{ddH_i} = \frac{m_d}{v_2} O_{2i}, \quad (26)$$

where $m_{u,d}$ denote the up- and down-type quark masses. Since we focus on the DM–quark scattering, the lepton sector is omitted. The trilinear scalar interactions involving the DM field χ are written as

$$-\mathcal{L} \supset C_{\chi\chi H_i} H_i \chi^2, \quad (27)$$

where

$$C_{\chi\chi H_i} = C_{\chi\chi h_1} O_{1i} + C_{\chi\chi h_2} O_{2i} + C_{\chi\chi s} O_{3i}. \quad (28)$$

Explicit expressions of these couplings are given by

$$C_{\chi\chi h_1} = \frac{\delta_1}{4} v_1, \quad C_{\chi\chi h_2} = \frac{\delta_2}{4} v_2, \quad C_{\chi\chi s} = \frac{d_2}{4} v_S. \quad (29)$$

In direct detection experiments, the squared momentum transfer $t \equiv (p_1 - p_3)^2$ is much smaller than the mediator masses, $t \ll m_{H_i}^2$. Under this approximation, the amplitudes for up- and down-type quarks become

$$\begin{aligned} i\mathcal{M}_{\text{up}} &= 2i \bar{u}(p_4) u(p_2) \frac{m_u}{v_2} \sum_{i=1}^3 \frac{C_{\chi\chi H_i} O_{2i}}{m_{H_i}^2} \\ &= 2i \bar{u}(p_4) u(p_2) \frac{m_u}{v_2} \sum_{i=1}^3 \left(C_{\chi\chi h_1} \frac{O_{1i} O_{2i}}{m_{H_i}^2} + C_{\chi\chi h_2} \frac{O_{2i}^2}{m_{H_i}^2} + C_{\chi\chi s} \frac{O_{3i} O_{2i}}{m_{H_i}^2} \right), \end{aligned} \quad (30)$$

$$i\mathcal{M}_{\text{down}} = 2i \bar{u}(p_4) u(p_2) \frac{m_d}{v_2} \sum_{i=1}^3 \left(C_{\chi\chi h_1} \frac{O_{1i} O_{2i}}{m_{H_i}^2} + C_{\chi\chi h_2} \frac{O_{2i}^2}{m_{H_i}^2} + C_{\chi\chi s} \frac{O_{3i} O_{2i}}{m_{H_i}^2} \right). \quad (31)$$

If the three Higgs boson masses are degenerate, the orthogonality of the mixing matrix implies

$$\sum_i O_{1i} O_{2i} = 0, \quad \sum_i O_{3i} O_{2i} = 0,$$

so the terms proportional to $O_{1i}O_{2i}$ and $O_{3i}O_{2i}$ cancel exactly. The only surviving contribution is the one proportional to O_{2i}^2 , whose size is controlled by

$$C_{\chi\chi h_2} = \frac{\delta_2}{4} v_2. \quad (32)$$

The coefficient δ_2 is given by Eq. (18), and is suppressed because the sum $\sum_i O_{2i}O_{3i}m_{H_i}^2$ becomes small due to the orthogonality of the mixing matrix. Hence, in the degenerate scalar limit, the entire amplitude becomes strongly suppressed. This orthogonality-induced suppression of δ_2 is the essential ingredient of the degenerate scalar scenario. However, if either v_2 or v_S is too small, δ_2 cannot be reduced, and the mechanism may cease to be effective. In Type-X Yukawa interactions, the same δ_2 -suppression pattern persists. In Type-II and Type-Y, on the other hand, the up-type (down-type) quarks couple with Φ_2 (Φ_1). Following a similar discussion, both Type-II and Type-Y require not only δ_2 -suppression, but also δ_1 -suppression. For a more detailed discussion, see ref. [12].

We also comment on an important phenomenological aspect of the degenerate scalar scenario relevant for Higgs searches at the LHC. In the 2HDMS, the couplings of the neutral Higgs bosons H_i to the SM final state X are given by the corresponding SM Higgs coupling multiplied by the mixing factor O_{1i} . The partial decay widths of H_i can be written as

$$\Gamma(H_1 \rightarrow XX) = \Gamma_{h \rightarrow XX}^{\text{SM}}(m_{H_1}) O_{11}^2, \quad (33)$$

$$\Gamma(H_2 \rightarrow XX) = \Gamma_{h \rightarrow XX}^{\text{SM}}(m_{H_2}) O_{12}^2, \quad (34)$$

$$\Gamma(H_3 \rightarrow XX) = \Gamma_{h \rightarrow XX}^{\text{SM}}(m_{H_3}) O_{13}^2, \quad (35)$$

where $\Gamma_{h \rightarrow XX}^{\text{SM}}(m_{H_i})$ denotes the SM Higgs decay width evaluated at m_{H_i} . If the three Higgs bosons are nearly degenerate around the observed Higgs mass, $m_{H_i} \simeq m_h = 125$ GeV, their combined decay width becomes

$$\Gamma(H_1 \rightarrow XX) + \Gamma(H_2 \rightarrow XX) + \Gamma(H_3 \rightarrow XX) \simeq \Gamma_{h \rightarrow XX}^{\text{SM}}(m_h), \quad (36)$$

because of the orthogonality relation $\sum_{i=1}^3 O_{1i}^2 = 1$. Consequently, the inclusive Higgs signal rate remains indistinguishable from the SM prediction for any values of the mixing angles, and the individual states H_i cannot be resolved with the current LHC sensitivity.

III. TREE-LEVEL MPP AND EWPT

In this section, we discuss the application of the MPP to the 2HDMS at the tree level and examine its implications for the EWPT. The MPP requires the coexistence of multiple vacua with identical energy densities. While the original idea of the MPP was formulated between the electroweak and a high-energy vacuum in the SM [13–15], in the present model, the scalar potential naturally possesses two distinct vacua at the low-energy scale: one along the electroweak direction and the other along the singlet direction. We therefore impose the tree-level MPP condition, which requires these two vacua to be degenerate in energy, as proposed in Ref. [17]. This condition serves as a basis for examining possible implications for the degenerate scalar scenario and the EWPT.

The classical background fields of the Higgs doublets and the singlet are parameterized as

$$\langle \Phi_i \rangle = \frac{1}{\sqrt{2}} \begin{pmatrix} 0 \\ \varphi_i \end{pmatrix}, \quad \langle S \rangle = \frac{\varphi_S}{\sqrt{2}}. \quad (37)$$

The tree-level potential in Eq. (1) can then be expressed in terms of these background fields as

$$\begin{aligned} V_0(\varphi_1, \varphi_2, \varphi_S) = & \frac{m_1^2}{2} \varphi_1^2 + \frac{m_2^2}{2} \varphi_2^2 - m_3^2 \varphi_1 \varphi_2 + \frac{\lambda_1}{8} \varphi_1^4 + \frac{\lambda_2}{8} \varphi_2^4 + \frac{\lambda_{345}}{4} (\varphi_1 \varphi_2)^2 \\ & + \frac{\delta_1}{8} \varphi_1^2 \varphi_S^2 + \frac{\delta_2}{8} \varphi_2^2 \varphi_S^2 + \frac{b_2}{4} \varphi_S^2 + \frac{d_2}{16} \varphi_S^4 + \sqrt{2} a_1 \varphi_S + \frac{b_1}{4} \varphi_S^2. \end{aligned} \quad (38)$$

The pattern of the EWPT in the 2HDMS corresponds to the transition from the singlet vacuum $(0, 0, v'_S)$ to the electroweak vacuum (v_1, v_2, v_S) . To discuss the EWPT, we work in the Landau gauge and assume that the charged scalar fields do not acquire VEVs at any temperature, so that the $U(1)_{\text{QED}}$ symmetry remains conserved.

The difference between the energy densities at the two vacua is expressed as

$$\begin{aligned} \Delta V_0 & \equiv V_0(v_1, v_2, v_S) - V_0(0, 0, v'_S) \\ & = \frac{m_1^2}{4} v_1^2 + \frac{m_2^2}{4} v_2^2 - \frac{m_3^2}{2} v_1 v_2 + \frac{3\sqrt{2}}{4} a_1 (v_S - v'_S) + \frac{1}{8} (b_1 + b_2) (v_S^2 - v'^2_S), \end{aligned} \quad (39)$$

where the tree-level MPP requires $\Delta V_0 = 0$. Electroweak symmetry breaking occurs when the quadratic coefficients m_1^2 and m_2^2 take negative values, leading to nonzero vacuum expectation values $v_{1,2}$. In our analysis, m_3^2 is treated as an input parameter and assumed to be

v	m_{H_1}	m_{H_2}	m_{H_3}	m_{H^\pm}	m_A	m_χ	α_1	α_2	α_3	$\tan \beta$	m_3^2
246.22	125.0	124.5	124.0	500	500	200	$\pi/4$	$\pi/4$	0.01	2.0	10

TABLE III. Input parameters adopted for the degenerate scalar scenario. The singlet VEV v_S and the linear parameter a_1 are treated as free parameters and scanned in the numerical analysis. The units of VEV and masses are GeV, while that of m_3^2 is GeV².

positive. Under these assumptions, the first three terms in Eq. (39) are negative. To realize the tree-level MPP, the fourth and fifth terms in Eq. (39) must compensate for this deficit. Since they scale with $(v_S - v'_S)$ and $(v_S^2 - v'^2_S) = (v_S - v'_S)(v_S + v'_S)$, a larger separation $|v_S - v'_S|$ tends to enhance their effect; the net sign, however, depends on a_1 and $b_1 + b_2$ (and on $v_S + v'_S$).

Two VEVs, v_S and v'_S , are obtained from the stationary conditions of the potential as

$$\begin{aligned} \frac{d_2}{2}v_S^3 + \left(b_1 + b_2 + \frac{\delta_1}{2}v_1^2 + \frac{\delta_2}{2}v_2^2 \right) v_S + 2\sqrt{2}a_1 &= 0, \\ \frac{d_2}{2}v'_S^3 + (b_1 + b_2)v'_S + 2\sqrt{2}a_1 &= 0. \end{aligned} \quad (40)$$

In the singlet vacuum, the Higgs doublets do not acquire VEVs, and therefore the terms proportional to $\delta_{1,2}$ are absent in the stationary condition. This difference between the two equations determines the distinct values of v_S and v'_S . Consequently, increasing $\delta_{1,2}$ tends to enlarge the separation between v_S and v'_S , which in turn facilitates the realization of $\Delta V_0 = 0$ under the tree-level MPP condition.

The mixing parameters $\delta_{1,2}$ are given in terms of the mass eigenvalues and the mixing matrix by Eqs. (17) and (18). In the degenerate scalar scenario, the combinations $\sum_{i=1}^3 O_{1i}O_{3i}m_{H_i}^2$ and $\sum_{i=1}^3 O_{2i}O_{3i}m_{H_i}^2$ become suppressed due to the orthogonality of the mixing matrix and the near degeneracy among the scalar masses. Therefore, obtaining large values of $\delta_{1,2}$ requires a relatively small singlet VEV v_S , since v_1 and v_2 are fixed by $v_1^2 + v_2^2 = v^2$ and cannot be reduced.

Before presenting the numerical results for the tree-level MPP condition, we show the parameter setup adopted for the degenerate scalar scenario. Representative values consistent with the degenerate scalar scenario and phenomenological constraints are summarized in Table III. The masses of the three Higgs bosons, m_{H_i} , are degenerate within 1 GeV. As discussed in Sec. II B, when the Higgs masses are nearly degenerate, the mixing angles α_i

are not strongly constrained.

In the following analysis, we adopt the Type-I Yukawa structure, in which all fermions couple to the same Higgs doublet Φ_2 . Experimental constraints are primarily associated with electroweak precision data and flavor observables. By assuming a mass degeneracy between the charged scalar H^\pm and either the neutral scalar H or the pseudoscalar A , i.e., $m_{H^\pm} \simeq m_H$ or m_A , the electroweak precision data can be satisfied [29]. In the Type-I 2HDMs, the process $B_d \rightarrow \mu^+ \mu^-$ requires $\tan \beta \gtrsim 1.75$ for $m_{H^\pm} = 500$ GeV [30]. We note that Higgs coupling measurements usually constrain $\cos(\beta - \alpha)$; however, this constraint does not apply in our analysis because it is based on the degenerate scalar scenario.

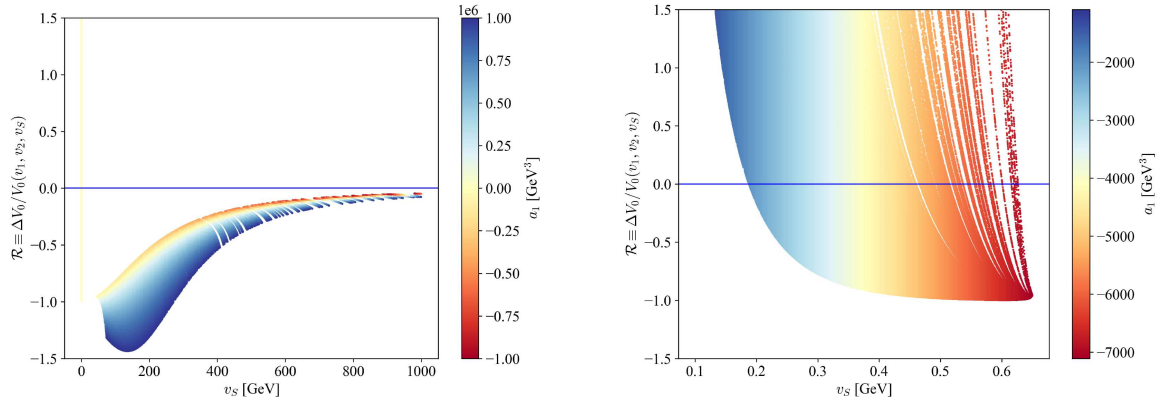


FIG. 1. Numerical results for $\mathcal{R} \equiv \Delta V_0/V_0(v_1, v_2, v_S)$ as a function of the singlet VEV v_S , where the color indicates the value of the soft-breaking parameter a_1 . The left panel corresponds to $0 < v_S < 1000$ GeV, while the right panel focuses on the region with $v_S \lesssim 0.7$ GeV.

Fig. 1 shows the numerical results for $\mathcal{R} \equiv \Delta V_0/V_0(v_1, v_2, v_S)$ as a function of the singlet VEV v_S , with the color indicating the soft breaking parameter a_1 . In the left panel, a few points approach and slightly cross the $\mathcal{R} = 0$ line only in the region with very small v_S , while no such points appear for larger v_S . The right panel enlarges this small- v_S region, making the behavior near $\mathcal{R} = 0$ more visible. Note that the range of the parameter a_1 differs between the left and right panels. As explained earlier, realizing the tree-level MPP condition requires large mixing parameters $\delta_{1,2}$, which are enhanced for smaller v_S . Consequently, solutions close to $\mathcal{R} = 0$ appear exclusively at small v_S , as clearly seen in the figure.

We also comment on the behavior of the color distribution in the small- v_S region of Fig. 1. d_2 is dominated by the term proportional to a_1/v_S^3 , as seen from Eq. (19). Since the

theoretical constraints require $0 < d_2 < 4\pi$, a small value of v_S forces a_1 to fall within a very narrow range. Therefore, in the small- v_S region, a_1 is almost uniquely determined by the value of v_S , which is why the color distribution in the right panel appears well aligned for small v_S .

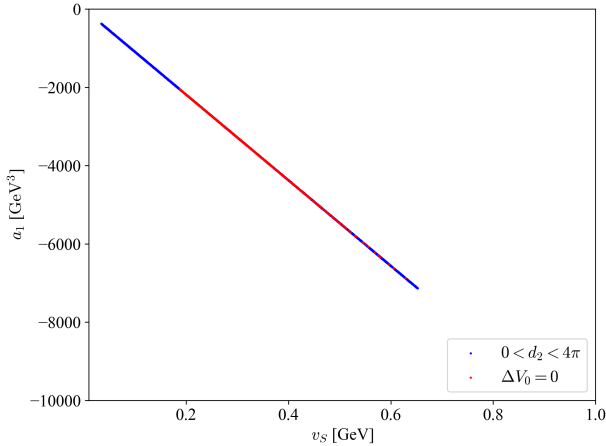


FIG. 2. Parameter points in the (v_S, a_1) plane. Blue points satisfy the theoretical constraint $0 < d_2 < 4\pi$, while red points additionally fulfill the tree-level MPP condition $\Delta V_0 = 0$.

To further illustrate this behavior, Fig. 2 shows the parameter points in the (v_S, a_1) plane. The blue points represent the region satisfying the theoretical constraint $0 < d_2 < 4\pi$, while the red points indicate the subset of these points that also fulfill the tree-level MPP condition $\Delta V_0 = 0$. For small values of v_S , the allowed points align approximately along a straight line, reflecting the fact that d_2 is dominated by the term proportional to a_1/v_S^3 . As v_S increases, however, the MPP condition itself ceases to be satisfied, even though the theoretical bound $0 < d_2 < 4\pi$ can still be fulfilled. This shows that the MPP requirement provides a stronger restriction on the parameter space than the perturbativity bound on d_2 , effectively setting an upper limit on v_S in the degenerate scalar scenario.

Before closing this section, we comment on the implications for the EWPT. A strong first-order EWPT, which is required for successful electroweak baryogenesis (EWBG), is commonly characterized by the condition [31–33]

$$\frac{v_C}{T_C} \gtrsim 1, \quad (41)$$

where T_C denotes the critical temperature at which the finite-temperature effective potential develops two degenerate minima, and v_C is the Higgs vacuum expectation value at $T = T_C$.

In the 2HDM_S, a first-order EWPT can, in principle, originate from two distinct sources: (i) the structure of the tree-level scalar potential, and (ii) thermal loop effects that generate cubic terms in the finite-temperature effective potential. However, once the tree-level MPP condition is imposed, the electroweak and singlet vacua become exactly degenerate at zero temperature. As a consequence, the tree-level potential does not develop an energy barrier between the two phases, and a tree-level-induced first-order EWPT is not possible in the MPP setup.

In this situation, a first-order EWPT can arise only from thermal loop effects. In the full one-loop finite-temperature effective potential, bosonic thermal contributions generate cubic terms that can induce an energy barrier between the symmetric and broken phases, potentially leading to a strong first-order EWPT. For completeness, the finite-temperature effective potential employed in our analysis is given by

$$V_{\text{eff}}(\varphi_1, \varphi_2, \varphi_S; T) = V_0(\varphi_1, \varphi_2, \varphi_S) + \sum_i n_i \left[V_{\text{CW}}(\bar{m}_i^2) + \frac{T^4}{2\pi^2} I_{B,F} \left(\frac{\bar{m}_i^2}{T^2} \right) \right], \quad (42)$$

where n_i is the number of degrees of freedom of particle i , V_{CW} denotes the Coleman–Weinberg potential, and $I_{B,F}$ are the thermal functions for bosons and fermions, respectively.

Finally, we note an important point regarding parameter dependence. The tree-level MPP condition favors large values of the mixing parameters $\delta_{1,2}$, since they enhance the separation between v_S and v'_S and help realize $\Delta V_0 = 0$. In contrast, the degenerate scalar scenario discussed in Sec. II B requires $\delta_{1,2}$ to be sufficiently small in order to suppress the DM-nucleon scattering amplitude. These two requirements therefore act in opposite directions, making their compatibility highly nontrivial. In the next section, we investigate this interplay by exploring concrete benchmark points.

IV. DM PHENOMENOLOGY

We now turn to the DM phenomenology of the 2HDM_S. In this section, we investigate whether the parameter points that satisfy the tree-level MPP condition, as studied in Sec. III, can also accommodate the results of the DM experiments. We select several representative benchmark points that satisfy the MPP condition and examine their predictions for the DM relic abundance and the spin-independent DM-nucleon scattering cross section.

The benchmark points are summarized in Table IV. First, we fix the three Higgs boson

BP	Inputs							Outputs	
	m_{H_1} [GeV]	m_{H_2} [GeV]	m_{H_3} [GeV]	m_χ [GeV]	v_S [GeV]	a_1 [GeV 3]	δ_1	δ_2	
BP1	125.0	124.5	124.0	62.5	0.20	-2194.76	8.49	2.04	
BP2	125.0	124.5	124.0	62.5	0.40	-4411.71	4.22	1.01	
BP3	125.0	124.5	124.0	62.5	0.60	-6607.28	2.81	0.67	

TABLE IV. Benchmark points satisfying the tree-level MPP condition. The three Higgs boson masses to be nearly degenerate within 0.5 GeV. All other input parameters not shown in this table are fixed to the same values as those given in Table III.

masses to be nearly degenerate, with a 0.5 GeV separation, consistent with the degenerate scalar scenario. Next, motivated by the results in Fig. 1, we select three representative values of the singlet VEV v_S in the small- v_S region favored by the MPP condition. As seen in Fig. 2, imposing the tree-level MPP fixes the soft-breaking parameter a_1 almost uniquely once v_S is chosen. For each selected v_S , we therefore determine the corresponding value of a_1 that satisfies $\Delta V_0 = 0$, and compute the associated parameters $\delta_{1,2}$, which are crucial for the DM phenomenology and the MPP analysis. According to Eqs. (17) and (18), the mixing parameters $\delta_{1,2}$ scale as $1/v_S$; therefore, increasing v_S leads to a suppression of $\delta_{1,2}$.

The observed DM relic abundance reported by Planck [34] is

$$\Omega_{\text{DM}} h^2 = 0.1200 \pm 0.0012, \quad (43)$$

which provides an upper bound on the relic density of the singlet-like DM particle χ . For our numerical analysis, we employ the public code `micrOMEGAs` [35], which computes both the relic abundance of χ , $\Omega_\chi h^2$, and the spin-independent cross section σ_{SI} . As we will show below, in the parameter region favored by the MPP and the degenerate scalar scenario, the particle χ typically constitutes only a fraction of the total DM abundance, $\Omega_\chi < \Omega_{\text{DM}}$. In this case, the effective scattering rate in direct detection experiments must be rescaled by the fraction of χ in the Universe:

$$\tilde{\sigma}_{\text{SI}} = \left(\frac{\Omega_\chi}{\Omega_{\text{DM}}} \right) \sigma_{\text{SI}}. \quad (44)$$

This rescaled cross section is then compared with the current upper limits from the LZ experiment [11]. In computing the DM relic density and the DM–quark scattering cross section, we treat the DM mass m_χ as a free variable.

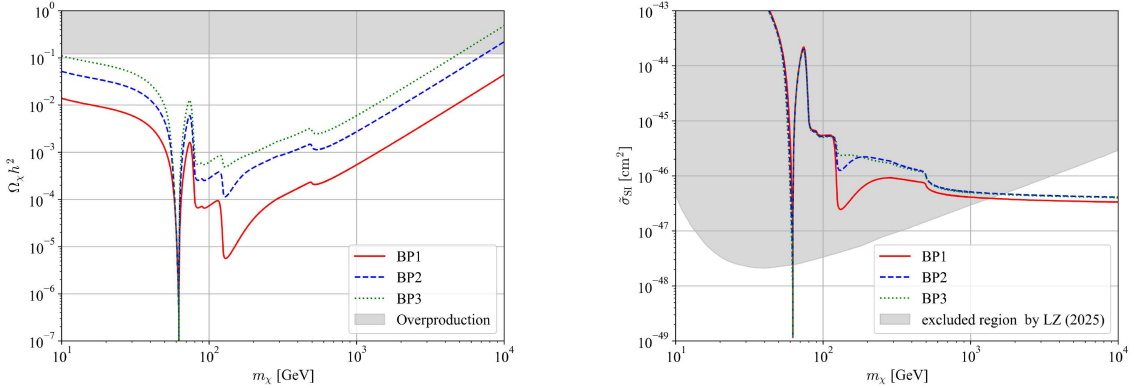


FIG. 3. Left: Relic abundance $\Omega_\chi h^2$ for BP1 (red solid), BP2 (blue dashed), and BP3 (green dotted). The gray-shaded region corresponds to DM overproduction. Right: Scaled spin-independent direct-detection cross section $\tilde{\sigma}_{\text{SI}}$ (see Eq. (44)) for the same benchmark points. The gray shaded region is excluded by the LZ experiment [11].

Fig. 3 shows the relic abundance (left) and the scaled spin-independent DM–nucleon scattering cross section (right) as functions of the DM mass m_χ . As seen in the left panel, the size of the relic abundance is strongly correlated with the mixing parameters $\delta_{1,2}$ (See Table IV). For BP1, where $\delta_{1,2}$ takes relatively large values, the DM annihilation cross section is enhanced, and the relic abundance is significantly reduced compared with BP2 and BP3. The sharp dip around $m_\chi \simeq m_{H_i}/2 \simeq 62.5$ GeV corresponds to the s -channel Higgs-resonant annihilation.

The right panel of Fig. 3 shows the scaled scattering cross section $\tilde{\sigma}_{\text{SI}}$ and therefore reflects the shape of the relic density curve. At first sight, it may seem surprising that the direct-detection rate is not strongly suppressed, despite the use of the degenerate scalar scenario discussed in Sec. II B. The reason is that the suppression mechanism relies on small values of $\delta_{1,2}$, whereas the tree-level MPP condition favors larger $\delta_{1,2}$ in order to enhance the separation between v_S and v'_S and realize $\Delta V_0 = 0$. Thus, the requirements for $\delta_{1,2}$ from the degenerate scalar scenario and from the MPP act in opposite directions.

In the previous subsection, we examined benchmark points in which the three neutral Higgs bosons were nearly degenerate with mass differences of about 0.5 GeV. These points satisfy the tree-level MPP condition, but do not fully realize the suppression mechanism of the degenerate scalar scenario, since the MPP prefers relatively large values of $\delta_{1,2}$.

BP	Inputs							Outputs	
	m_{H_1} [GeV]	m_{H_2} [GeV]	m_{H_3} [GeV]	m_χ [GeV]	v_S [GeV]	a_1 [GeV 3]	δ_1	δ_2	
BP4	125.0	124.5	124.0	62.5	0.63	-6867.62	2.71	0.65	
BP5	125.0	124.75	124.5	62.5	0.31	-3388.83	2.77	0.66	
BP6	125.0	124.9	124.8	62.5	0.12	-1376.29	2.74	0.66	

TABLE V. Benchmark points with increasingly degenerate neutral scalar masses. The mass differences among H_1 , H_2 , and H_3 are 0.50 GeV (BP4), 0.25 GeV (BP5), and 0.10 GeV (BP6), respectively. All other input parameters not shown in this table are fixed to the same values as those given in Table III.

A natural question is therefore whether a stronger mass degeneracy among the Higgs bosons could improve the situation. To address this, we introduce additional benchmark points, BP4, BP5, and BP6, shown in Table V. Here, the Higgs masses are chosen to be more tightly clustered, with differences reduced to 0.50 GeV (BP4), 0.25 GeV (BP5), and 0.10 GeV (BP6). As can be seen from Table V, the resulting values of the mixing parameters $\delta_{1,2}$ are almost identical for BP4, BP5, and BP6. This is because, for each choice of the Higgs mass difference, the singlet VEV v_S is chosen to be as large as possible while still satisfying the tree-level MPP condition. Such a choice effectively corresponds to selecting the minimal values of $\delta_{1,2}$ compatible with the MPP. Indeed, from Eqs. (17) and (18), once $\delta_{1,2}$ are fixed, the singlet VEV v_S is uniquely determined for a given pattern of Higgs mass differences. As a result, increasing the degree of mass degeneracy does not provide additional freedom to reduce $\delta_{1,2}$ when the MPP condition is imposed.

The relic abundance and direct detection predictions for BP4, BP5, and BP6 are shown in Fig. 4. As discussed above, since the mixing parameters $\delta_{1,2}$ take almost identical values for BP4, BP5, and BP6, the corresponding curves in Fig. 4 nearly overlap and are hardly distinguishable. As a result, increasing the level of mass degeneracy does not lead to additional suppression of the DM scattering amplitude.

It is worth emphasizing that viable parameter space remain. Two regions allow simultaneous satisfaction of the tree-level MPP condition, the DM relic abundance requirement, and the DM direct detection constraint: (i) the resonance region near $m_\chi \simeq 62.5$ GeV, and (ii) the heavy mass regime with $m_\chi = \mathcal{O}(1\text{--}10)$ TeV. These regions provide concrete

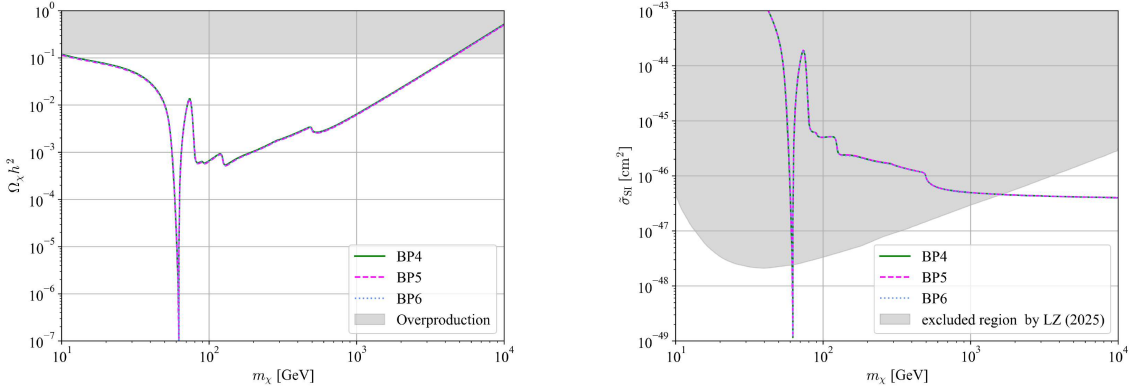


FIG. 4. Left: Relic abundance $\Omega_\chi h^2$ for BP4 (green solid), BP5 (magenta dashed), and BP6 (light blue dotted). The gray-shaded region corresponds to DM overproduction. Right: Scaled spin-independent direct-detection cross section $\tilde{\sigma}_{\text{SI}}$ (see Eq. (44)) for the same benchmark points. The gray shaded region is excluded by the LZ experiment [11].

	BP1	BP2	BP3	BP4	BP5	BP6
v_C/T_C	$\frac{237.9}{69.7} = 3.4$	$\frac{237.9}{69.7} = 3.4$	$\frac{237.9}{69.7} = 3.4$	$\frac{238.2}{68.4} = 3.5$	$\frac{238.1}{69.1} = 3.4$	$\frac{238.0}{69.5} = 3.4$

TABLE VI. Ratio v_C/T_C at the critical temperature for BP1–BP6, evaluated using `CosmoTransitions` [36]. The Parwani resummation method [37] is used in this analysis.

examples in which the MPP and DM phenomenology can be compatible within the 2HDMS.

Finally, we comment on the strength of the EWPT at the quantitative level. The calculations are carried out using `CosmoTransitions` [36], based on the one-loop finite-temperature effective potential given in Eq. (42). At finite temperature, however, bosonic multi-loop contributions can spoil the validity of naive perturbation theory. To properly account for these effects, thermal resummation is required. In this work, we adopt the Parwani resummation scheme [37], in which thermal corrections are incorporated by resumming all Matsubara frequency modes. In a tree-level-driven first-order EWPT, the strength of the transition is highly sensitive to the mixing parameters $\delta_{1,2}$, which control the structure of the tree-level potential. However, in the present setup, the tree-level MPP condition is imposed, and therefore, a tree-level-induced first-order phase transition does not occur.

Instead, the first-order EWPT is generated by thermal loop effects at the one-loop level as discussed in Sec. III. In this case, the dominant contribution to the cubic term in the finite-

temperature effective potential arises from bosonic thermal loops, and the strength of the transition is mainly controlled by the bosonic mass spectrum. Since our benchmark points are chosen in a region where the scalar masses are nearly degenerate, there is no significant variation in the relevant bosonic masses among BP1–BP6. As a result, the values of v_C/T_C show only mild differences across the benchmark point as shown in Table VI. We find that all benchmark points satisfy the condition for a strong first-order EWPT in Eq. (41).

V. SUMMARY

In this work, we have studied the 2HDMS, focusing on the implications of imposing the tree-level MPP. The scalar potential of the model naturally possesses two distinct vacua along the electroweak and singlet directions, and we required these vacua to be degenerate at tree level. This tree-level MPP condition fixes a nontrivial relation among the parameters. We demonstrated that the MPP requirement favors large values of the mixing parameters $\delta_{1,2}$, because they enhance the separation between v_S and v'_S and enable the realization of $\Delta V_0 = 0$.

The imaginary component of the singlet field serves as a stable WIMP DM candidate. Its interactions with nucleons arise from t -channel exchange of the three neutral Higgs bosons $H_{1,2,3}$. When the masses of these scalars are nearly degenerate, the orthogonality of the mixing matrix leads to cancellations among the scattering amplitudes, naturally suppressing the spin-independent DM-quark cross section. This mechanism, known as the degenerate scalar scenario, offers a compelling way to satisfy stringent direct detection constraints. However, the degenerate scalar scenario requires the mixing parameters $\delta_{1,2}$ to be sufficiently small for the amplitude cancellation to be effective. As a result, the MPP and the degenerate scalar scenario impose mutually competing requirements on $\delta_{1,2}$, making their simultaneous realization highly nontrivial.

We explored this tension by constructing explicit benchmark points that satisfy the tree-level MPP condition. The tree-level MPP requires large values of the mixing parameters $\delta_{1,2}$, and achieving such values in turn demands a small singlet VEV v_S . As anticipated, this makes the suppression mechanism of the degenerate scalar scenario less effective. To examine whether stronger mass degeneracy could improve the situation, we further considered cases in which the neutral Higgs bosons are even more tightly degenerate in mass. However,

the MPP effectively fixes v_S for a given pattern of mass differences, thereby determining the size of $\delta_{1,2}$. As a consequence, increasing the level of mass degeneracy does not lead to additional suppression of the DM direct-detection rate. Nevertheless, we found that two parameter regions remain in which all constraints can be satisfied simultaneously: (i) the Higgs-resonance region with $m_\chi \simeq 62.5$ GeV, and (ii) the heavy-mass regime with $m_\chi = \mathcal{O}(1\text{--}10)$ TeV.

We also examined the implications of the tree-level MPP for the EWPT. Although the MPP forbids a tree-level-driven first-order transition due to the exact vacuum degeneracy at zero temperature, we found that thermal loop effects at the one-loop level can still generate a strong first-order EWPT. Indeed, all benchmark points considered in this work satisfy the conventional criterion for a strong first-order EWPT.

To summarize, imposing the tree-level MPP strongly constrains the structure of the scalar potential, most notably by requiring the mixing parameters $\delta_{1,2}$ to be large. In contrast, the degenerate scalar scenario introduced to suppress the DM spin-independent scattering rate essentially requires the same parameters $\delta_{1,2}$ to be sufficiently small. Thus, the tree-level MPP and the degenerate scalar scenario impose mutually conflicting demands on $\delta_{1,2}$, making their simultaneous realization highly nontrivial. Nevertheless, in this work, we have shown that viable parameter regions remain, in which the results of the DM experiments are reproduced while a strong first-order EWPT can still be achieved.

ACKNOWLEDGMENTS

The work of GCC is supported by JSPS KAKENHI Grant No. 22K03616. The work of CI is supported by the National Natural Science Foundation of China (NNSFC) Grant No.12475111.

Appendix A: Input and output parameters

The following shows the relationship between the input and output parameters described in Table I except for δ_1 , δ_2 and d_2 .

$$m_1^2 = \frac{m_3^2 v_2}{v_1} - \frac{\lambda_1 v_1^2}{2} - \frac{\lambda_{345} v_2^2}{2} - \frac{\delta_1 v_S^2}{4}, \quad (\text{A1})$$

$$m_2^2 = \frac{m_3^2 v_1}{v_2} - \frac{\lambda_2 v_2^2}{2} - \frac{\lambda_{345} v_1^2}{2} - \frac{\delta_2 v_S^2}{4}, \quad (\text{A2})$$

$$\lambda_1 = \frac{1}{v_1^2} \left(\sum_{i=1}^3 O_{1i}^2 m_{H_i}^2 - \frac{m_3^2 v_2}{v_1} \right), \quad (\text{A3})$$

$$\lambda_2 = \frac{1}{v_2^2} \left(\sum_{i=1}^3 O_{2i}^2 m_{H_i}^2 - \frac{m_3^2 v_1}{v_2} \right), \quad (\text{A4})$$

$$\lambda_3 = \frac{1}{v_1 v_2} \left(\sum_{i=1}^3 O_{1i} O_{2i} m_{H_i}^2 + m_3^2 \right) - \lambda_4 - \lambda_5, \quad (\text{A5})$$

$$\lambda_4 = \frac{2}{v^2} \left(\frac{m_3^2}{\sin \beta \cos \beta} - m_{H^\pm}^2 \right) - \lambda_5, \quad (\text{A6})$$

$$\lambda_5 = \frac{1}{v^2} \left(\frac{m_3^2}{\sin \beta \cos \beta} - m_A^2 \right), \quad (\text{A7})$$

$$b_2 = \frac{-4\sqrt{2}a_1 - 2b_1 v_S - \delta_1 v_1^2 v_S - \delta_2 v_2^2 v_S - d_2 v_S^3}{2v_S}, \quad (\text{A8})$$

$$b_1 = -m_\chi^2 - \frac{\sqrt{2}a_1}{v_S}. \quad (\text{A9})$$

[1] G. Aad *et al.* (ATLAS), *Phys. Lett. B* **716**, 1 (2012), arXiv:1207.7214 [hep-ex].

[2] S. Chatrchyan *et al.* (CMS), *Phys. Lett. B* **716**, 30 (2012), arXiv:1207.7235 [hep-ex].

[3] T. D. Lee, *Phys. Rev. D* **8**, 1226 (1973).

[4] S. L. Glashow and S. Weinberg, *Phys. Rev. D* **15**, 1958 (1977).

[5] N. G. Deshpande and E. Ma, *Phys. Rev. D* **18**, 2574 (1978).

[6] G. C. Branco, P. M. Ferreira, L. Lavoura, M. N. Rebelo, M. Sher, and J. P. Silva, *Phys. Rept.* **516**, 1 (2012), arXiv:1106.0034 [hep-ph].

[7] X.-M. Jiang, C. Cai, Z.-H. Yu, Y.-P. Zeng, and H.-H. Zhang, *Phys. Rev. D* **100**, 075011 (2019), arXiv:1907.09684 [hep-ph].

[8] Z. Zhang, C. Cai, X.-M. Jiang, Y.-L. Tang, Z.-H. Yu, and H.-H. Zhang, *JHEP* **05**, 160 (2021), arXiv:2102.01588 [hep-ph].

[9] T. Biekötter and M. O. Olea-Romacho, *JHEP* **10**, 215 (2021), arXiv:2108.10864 [hep-ph].

[10] T. Biekötter, P. Gabriel, M. O. Olea-Romacho, and R. Santos, *JHEP* **10**, 126 (2022), arXiv:2207.04973 [hep-ph].

[11] J. Aalbers *et al.* (LZ), (2024), arXiv:2410.17036 [hep-ex].

[12] G.-C. Cho and C. Idegawa, *PTEP* **2025**, 023B04 (2025), arXiv:2410.14328 [hep-ph].

[13] D. L. Bennett and H. B. Nielsen, *Int. J. Mod. Phys. A* **9**, 5155 (1994), arXiv:hep-ph/9311321.

[14] D. L. Bennett and H. B. Nielsen, *Int. J. Mod. Phys. A* **14**, 3313 (1999), arXiv:hep-ph/9607278.

[15] D. L. Bennett, *Multiple point criticality, nonlocality, and fine tuning in fundamental physics: Predictions for gauge coupling constants gives alpha**-1 = 136.8 +- 9*, Ph.D. thesis (1996), arXiv:hep-ph/9607341.

[16] C. D. Froggatt and H. B. Nielsen, *Phys. Lett. B* **368**, 96 (1996), arXiv:hep-ph/9511371.

[17] K. Kannike, N. Koivunen, and M. Raidal, *Nucl. Phys. B* **968**, 115441 (2021), arXiv:2010.09718 [hep-ph].

[18] V. A. Kuzmin, V. A. Rubakov, and M. E. Shaposhnikov, *Phys. Lett.* **155B**, 36 (1985).

[19] G.-C. Cho, C. Idegawa, and R. Sugihara, *Phys. Lett. B* **839**, 137757 (2023), arXiv:2212.13029 [hep-ph].

[20] S. Nie and M. Sher, *Phys. Lett. B* **449**, 89 (1999), arXiv:hep-ph/9811234.

[21] S. Kanemura, T. Kasai, and Y. Okada, *Phys. Lett. B* **471**, 182 (1999), arXiv:hep-ph/9903289.

[22] S. Kanemura, T. Kubota, and E. Takasugi, *Phys. Lett. B* **313**, 155 (1993), arXiv:hep-ph/9303263.

[23] A. G. Akeroyd, A. Arhrib, and E.-M. Naimi, *Phys. Lett. B* **490**, 119 (2000), arXiv:hep-ph/0006035.

[24] I. F. Ginzburg and I. P. Ivanov, *Phys. Rev. D* **72**, 115010 (2005), arXiv:hep-ph/0508020.

[25] C.-Y. Chen, S. Dawson, and I. M. Lewis, *Phys. Rev. D* **91**, 035015 (2015), arXiv:1410.5488 [hep-ph].

[26] K. R. Maleki and K. Ghorbani, (2022), arXiv:2211.12102 [hep-ph].

[27] M. Aoki, T. Komatsu, and H. Shibuya, *PTEP* **2022**, 063B05 (2022), arXiv:2106.03439 [hep-ph].

[28] E. A. Paschos, *Phys. Rev. D* **15**, 1966 (1977).

[29] H. E. Haber and D. O’Neil, *Phys. Rev. D* **83**, 055017 (2011), arXiv:1011.6188 [hep-ph].

[30] J. Haller, A. Hoecker, R. Kogler, K. Mönig, T. Peiffer, and J. Stelzer, *Eur. Phys. J. C* **78**, 675 (2018), arXiv:1803.01853 [hep-ph].

- [31] P. B. Arnold and L. D. McLerran, *Phys. Rev. D* **36**, 581 (1987).
- [32] A. I. Bochkarev and M. E. Shaposhnikov, *Mod. Phys. Lett. A* **2**, 417 (1987).
- [33] K. Funakubo and E. Senaha, *Phys. Rev. D* **79**, 115024 (2009), arXiv:0905.2022 [hep-ph].
- [34] N. Aghanim *et al.* (Planck), *Astron. Astrophys.* **641**, A6 (2020), [Erratum: *Astron. Astrophys.* 652, C4 (2021)], arXiv:1807.06209 [astro-ph.CO].
- [35] G. Belanger, A. Mjallal, and A. Pukhov, *Eur. Phys. J. C* **81**, 239 (2021), arXiv:2003.08621 [hep-ph].
- [36] C. L. Wainwright, *Comput. Phys. Commun.* **183**, 2006 (2012), arXiv:1109.4189 [hep-ph].
- [37] R. R. Parwani, *Phys. Rev. D* **45**, 4695 (1992), [Erratum: *Phys. Rev. D* **48**, 5965 (1993)], arXiv:hep-ph/9204216.